Check for updates

Metal–Covalent Organic Frameworks

How to cite: *Angew. Chem. Int. Ed.* **2022**, *61*, e202204326
International Edition: doi.org/10.1002/anie.202204326
German Edition: doi.org/10.1002/ange.202204326

Nickel Glyoximate Based Metal–Covalent Organic Frameworks for Efficient Photocatalytic Hydrogen Evolution

Lishan Sun[+], Meng Lu[+], Zongfan Yang, Zhenyi Yu, Xi Su, Ya-Qian Lan, and Long Chen**

Abstract: Metal–covalent organic frameworks (MCOFs) have been recently received wide attention owing to the homogeneous distribution of active metal centers that are beneficial for enhancing the application potentials. However, metal complex based functional building blocks for MCOFs synthesis are limited. Herein, two new MCOFs (Ni-Py-COF and Ni-Bn-COF) were constructed via a novel nickel glyoximate based building block. Splendid photocatalytic activity on hydrogen evolution from water and great long-term recyclability were achieved using these nickel glyoximate based MCOFs as photocatalysts. Excitingly, even without the addition of Pt co-catalyst, the hydrogen evolution rates (HER) of Ni-Py-COF reached up to 626 $\mu mol\,g^{-1}\,h^{-1}$, which is better than many porous organic polymers. This work not only expands the type of building units for MCOFs, but also provides meaningful insights for developing stable, efficient and earth-abundant photocatalysts toward H_2 generation.

Covalent organic frameworks (COFs), as a promising class of porous crystalline polymers, have demonstrated considerable advantages and application potential in various fields owing to designable structures and tailor-made functions.[1] C, H, N and other light elements constituted the majority of COFs namely metal-free COFs.[2] However, most metal-free COFs fail to exhibit versatile and outstanding properties due to their limited constituent elements.[3] Recently, a new class of COFs with intentionally integrated metal centers into the skeletons are considered as promising candidates to address this dilemma; these are referred to as metal–covalent organic frameworks (MCOFs).[4] MCOFs not only inherit the merits of COFs including good crystallinity, permanent porosity, high stability and tunability, but also provide additional metal active sites and cooperative effects to achieve superior performance in catalysis,[5,9a] molecular adsorption and separation,[6] optoelectronics[7] and sensing.[8] The synthesis of MCOFs is largely dependent on the metal-coordinated molecules or complexes that serve as the building blocks.[4] However, the metalated precursors suitable for MCOFs synthesis are very rare, mainly limited in metallosalen/metallosalphen,[6a,9] metalloporphyrins,[5] metallophthalocyanines[7,8] and 2,2′-bipyridine (bpy) metal complexes.[6b] Therefore, it is particularly interesting and highly desirable to develop new metalated moieties for the construction of functional MCOFs.

With the continuous consumption of fossil fuels and the concurrent environmental problems, it is urgent to explore alternative and sustainable energy resources. Hydrogen is known as a kind of green energy with high energy density.[10] Photocatalytic water splitting for hydrogen production using the ubiquitous solar energy is a prospective technology, which aroused great attention.[11] Notably, a number of COFs demonstrated decent performance on light-driven H_2 evolution,[12] thanks to their designable structures, tunable energy levels and outstanding charge-transport properties. Increasing research efforts have been devoted to developing new photocatalytic COFs since the first report on a hydrazone-based COF used for photocatalytic H_2 evolution in 2014.[12a] On the other hand, to promote the separation of photo-excited charge carriers and decrease the overpotential of H_2 evolution, noble metals (Pt, Au, Ag) are necessary to be employed as co-catalysts,[12,13] which unfortunately impede the widespread applications of the technology due to the rarity and high cost. Thus, the exploration of cost-effective and earth-abundant alternative co-catalysts or avoiding using co-catalysts is of great significance.[14]

Metal glyoximate complexes have been investigated for more than a century (Scheme 1).[15] These complexes exhibit good stability and unique electronic properties originating from their planar structure and intramolecular hydrogen bonding.[16] The planar structure of metal glyoximate ligands is beneficial to form charge transfer salts featuring stacked 2D layered structures.[17] Therefore, metal glyoximate complexes are expected to be a potential non-noble-metal photocatalytic platform. And the analogues of nickel(II) glyoximate have been used as co-catalysts to enhance the H_2 evolution performance.[18] However, such post-modification methods preclude precise structural analysis, which are not conducive to unraveling the underlying catalytic mechanism. In 2020, Dincă group reported Ni glyoximate based metal–

[*] L. Sun,[+] Z. Yang, Dr. Z. Yu, X. Su, Prof. L. Chen
Department of Chemistry, Tianjin Key Laboratory of Molecular Optoelectronic Science, Tianjin University
Tianjin 300072 (China)
E-mail: long.chen@tju.edu.cn

Prof. L. Chen
State Key Laboratory of Supramolecular Structure and Materials, College of Chemistry, Jilin University
Changchun 130012 (China)
E-mail: longchen@jlu.edu.cn

Dr. M. Lu,[+] Prof. Y.-Q. Lan
School of Chemistry, South China Normal University
Guangzhou 510006 (China)
E-mail: yqlan@m.scnu.edu.cn

[+] These authors contributed equally to this work.

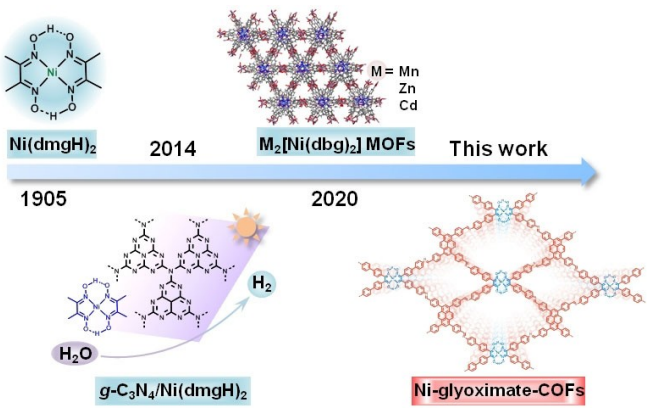

Scheme 1. The brief development of Ni glyoximate and related porous materials.

organic frameworks (MOFs) which featured excellent charge transport properties.[19] Herein, we directly integrate nickel glyoximate into the COF skeleton to realize stable recycling of the photocatalyst and better unraveling of the structure–activity relationship.

We firstly designed a C_4-symmetric nickel glyoximate building block ($Ni(dbpag)_2$) with tetraamine functional groups. Imine polycondensation of $Ni(dbpag)_2$ with two tetratopic aromatic aldehydes afforded corresponding nickel glyoximate based 2D MCOFs (Ni-glyoximate-COFs: Ni-Py-COF and Ni-Bn-COF). Furthermore, regarding the abundant and uniformly distributed nickel glyoximate cores in the framework, we systematically investigated their photocatalytic performance for hydrogen evolution. Therein, Ni-Py-COF exhibited superior performance, with a H_2 evolution rate (HER) of 13231 $\mu mol\,g^{-1}\,h^{-1}$ seven times higher than that of Ni-Bn-COF (1805 $\mu mol\,g^{-1}\,h^{-1}$). Excitingly, even without the addition of Pt co-catalyst, the HER of Ni-Py-COF reached up to 626 $\mu mol\,g^{-1}\,h^{-1}$, which is better than many porous organic polymers with Ni as co-catalyst.[18a,20] Furthermore, Ni-Py-COF showed good long-term cycling stability, which indicated that it was very promising in solar-driven water splitting. This work not only expands the library of MCOFs but also provides a viable approach toward photocatalytic hydrogen evolution without using noble metals.

Firstly, $Ni(dbpag)_2$ was newly synthesized (Scheme S2) and characterized by single-crystal X-ray diffraction analysis (Figure S15). And it was further condensed with two C_4-symmetric tetratopic aldehydes of 1,3,6,8-tetrakis(4-formylphenyl)pyrene (Py-4CHO) and 1,2,4,5-tetrakis-(4-formylphenyl)benzene (Bn-4CHO), respectively, which afforded two Ni glyoximate based COFs (Ni-Py-COF and Ni-Bn-COF) under solvothermal conditions in a mixed solvent of *o*-dichlorobenzene/isopropanol/AcOH at 120 °C for five days (Scheme 2).

Fourier transform infrared spectroscopies (FT-IR) and solid-state ^{13}C cross-polarization with total suppression of spinning sidebands (CP-TOSS) spectroscopies confirmed the chemical structures of two Ni-glyoximate-COFs. As revealed in the FT-IR spectra (Figure S9), the characteristic

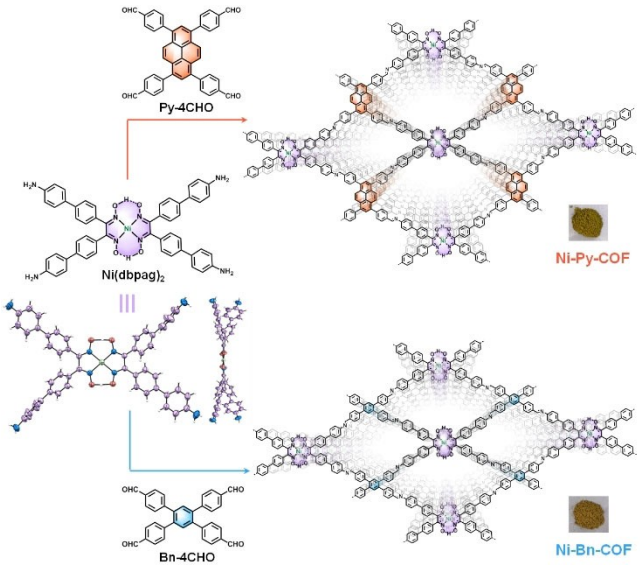

Scheme 2. Synthetic route of Ni-glyoximate-COFs.

N–H stretching bands (3357 and 3217 cm^{-1}) for the amine groups of the $Ni(dbpag)_2$ nearly disappeared and the C=O stretching bands at 1695 cm^{-1} from aldehyde monomers (Py-4CHO and Bn-4CHO) were dramatically decreased, which indicated high imine condensation efficiency. In addition, the stretching vibration peaks attributed to C=N linkages in Ni-glyoximate-COFs were observed at 1603 cm^{-1}. Besides, the formation of C=N bonds was also verified by ^{13}C CP-TOSS NMR. The chemical shifts around 152 ppm in the ssNMR spectra of both Ni-Py-COF and Ni-Bn-COF can be attributed to the carbon atoms of C=N bonds (Figure S10). X-ray photoelectron spectroscopy (XPS) was further performed to determine the metal electron valence states of Ni-glyoximate-COFs, and the results suggested Ni centers in both COFs were +2 oxidation state (Figures S11 and S12). Notably, the elemental contents of C, H, N and Ni for both Ni-glyoximate-COFs estimated by the elemental analysis and ICP-MS measurements were well consistent with the theoretical values (Table S1).

The crystalline structures of Ni-glyoximate-COFs were determined by powder X-ray diffraction (PXRD) measurements combined with structural simulation. As shown in Figures 1a and S16, an intensive diffraction peak at 4.25° was detected in the PXRD pattern for Ni-Py-COF, which was reasonably assigned to the (110) reflection together with other peaks at 2.92°, 6.76° and 8.43°, which could be indexed to the (100), (120) and (220) facets, respectively. Similarly, the PXRD profile of Ni-Bn-COF also exhibited similar diffraction peaks at 3.08°, 4.49°, 7.12° and 9.03°, which could be attributed to the (100), (110), (120) and (220) facets, respectively (Figures 1b and S17). The calculated diffraction patterns of both Ni-Py-COF and Ni-Bn-COF based on AA stacking model could reproduce the experimental data very well, while the simulated profile of AB stacking mode showcased a huge difference (Figures 1, S16 and S17). Furthermore, Pawley refinement was performed to optimize the unit cell parameters (a = 31.46 Å, b = 29.75 Å, c = 3.96 Å,

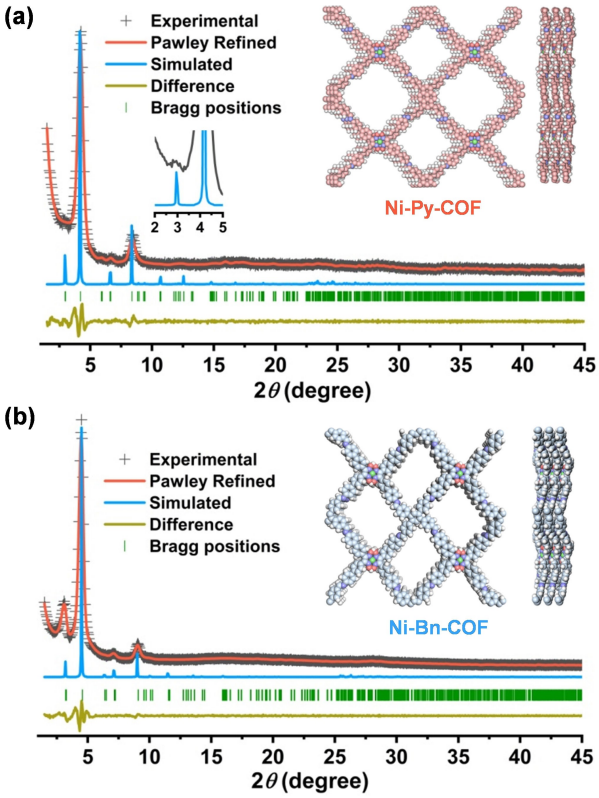

Figure 1. a) PXRD patterns of Ni-Py-COF, the insets show partial enlarged detail and its structure of AA stacking mode viewed top and side. b) PXRD patterns of Ni-Bn-COF, and the inset shows its structure of AA stacking mode viewed top and side.

$\alpha=\gamma=90°$, $\beta=73.36°$ for Ni-Py-COF; $a=27.97$ Å, $b=27.44$ Å, $c=3.53$ Å, $\alpha=\gamma=90°$, $\beta=89.36°$ for Ni-Bn-COF). Eventually, the final R_{wp} and R_p values converged to 4.22 %, 3.19 % for Ni-Py-COF, and 4.70 %, 3.70 % for Ni-Bn-COF, respectively, which resulted in satisfactorily low residual values and acceptable profile differences. Additionally, as revealed by scanning electron microscopy (SEM) images, Ni-Py-COF exhibited a rod-like morphology while Ni-Bn-COF adapted a spherical-like morphology (Figure S13). Transmission electron microscopy (TEM) images of both COFs showcased clear lattice stripes (Figure S14), which suggested that Ni-glyoximate-COFs feature high crystallinity and long-range ordered structures.

Nitrogen sorption and desorption measurements at 77 K were performed to evaluate the inherent porosities of both Ni-glyoximate-COFs. As shown in Figure 2, the nitrogen adsorption isotherm of both Ni-glyoximate-COFs revealed typical type-I isotherms, indicating their microporous characteristics. Ni-Py-COF and Ni-Bn-COF showcased comparable Brunauer–Emmett–Teller (BET) surface area of 1051 and 1240 $m^2 g^{-1}$, respectively. Based on the nonlocal density functional theory (NLDFT) method, the pore size distributions (PSD) were calculated to be 1.15 and 1.73 nm for Ni-Py-COF and 1.05 and 1.58 nm for Ni-Bn-COF, respectively, which were in good agreement of the theoretical values in the eclipsed (AA) model (Figures S16 and S17).

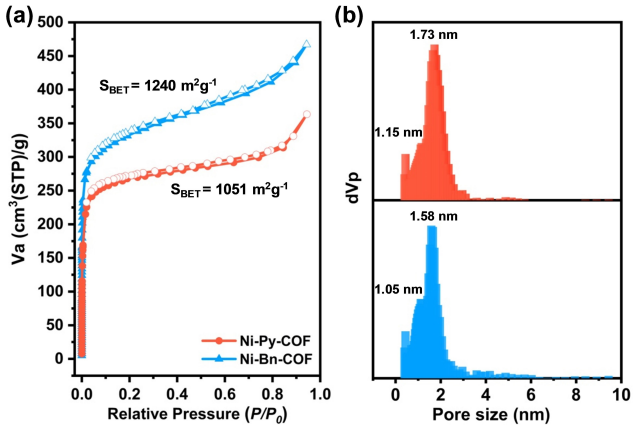

Figure 2. a) Nitrogen sorption isotherms and b) pore size distribution profiles of Ni-Py-COF (OrangeRed) and Ni-Bn-COF (DodgerBlue).

The chemical stability of two Ni-glyoximate-COFs were tested in different concentrations of acids and bases after soaking for 3 days at room temperature. As a result, both Ni-Py-COF and Ni-Bn-COF maintained their crystallinities and chemical structures after treatments in these harsh conditions, which was proved by PXRD and FT-IR measurements (Figures S18 and S19). Thermogravimetric analysis (TGA) indicated that both Ni-glyoximate-COFs could be stable up to ca. 290 °C which are probably caused by the decomposition of the Ni glyoximate core.[21] Provably, the TGA results of the model complex of bis(1,2-diphenylethanedionedioximato)nickel(II) ($Ni(dpg)_2$) showed that Ni glyoximate core could be stable up to ca. 290 °C under N_2 atmosphere (Figure S20). However, Ni-Py-COF and Ni-Bn-COF retain 67 % and 61 % of their initial mass at 800 °C separately (Figure S20). On the other hand, the results of water contact angle measurements proved that both Ni-glyoximate-COFs were superhydrophilic in which the droplets were fully impregnated about 1.23 s (Figure S21). All these results indicated that both Ni-glyoximate-COFs exhibited decent stability and superhydrophilic nature which are crucial for photocatalytic H_2 evolution.

The appropriate band structure is one of the most important parameters of catalysts for photocatalytic hydrogen production. The band gaps and electronic structures of both Ni-glyoximate-COFs were evaluated by UV/Vis diffuse reflectance spectroscopy (UV-DRS) and Mott–Schottky measurements. As displayed in Figure 3, both Ni-glyoximate-COFs exhibited similar optical absorption with the edge around 650 nm. The optical band gaps of Ni-Py-COF and Ni-Bn-COF were about 1.82 and 1.75 eV, respectively, calculated from the Tauc plots. Mott–Schottky (M–S) measurements were further conducted to explore the band positions of Ni-glyoximate-COFs (Figures 3c and S22). The results revealed that both Ni-glyoximate-COFs were *n*-type semiconductors because of the positive slopes. Their flat band potential (E_{fb}) were −1.30 and −1.24 V vs. Ag/AgCl of Ni-Py-COF and Ni-Bn-COF, respectively. It is known that the bottom of conduction band(CB) nearly equals to the E_{fb} in the *n*-type semiconductors,[22] so the CB of Ni-Py-COF

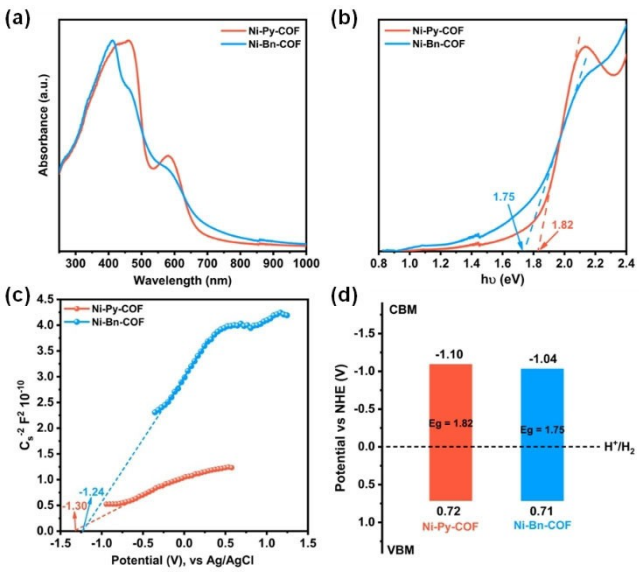

Figure 3. a) UV/Visible absorption spectrum of Ni-Py-COF (OrangeRed line) and Ni-Bn-COF (DodgerBlue line). b) Kubelka–Munk-transformed reflectance spectra upon visible light irradiation. c) Mott–Schottky plots for Ni-Py-COF (OrangeRed line) and Ni-Bn-COF (DodgerBlue line) at 1000 Hz frequency. d) Band structure diagram for Ni-glyoximate-COFs as determined from Mott–Schottky plots and UV-DRS.

and Ni-Bn-COF were around −1.10 and −1.04 V vs. normal hydrogen electrode (NHE), respectively, which showed more negative than the theoretical potential for H^+-to-H_2. The valence band (VB) positions were further deduced to be 0.72 and 0.71 V vs. NHE combining with band gap from UV-DRS (Figure 3d). These results verified that both Ni-glyoximate-COFs feature matched energy potentials and are feasible to activate the photocatalytic proton reduction from water.

To confirm the photocatalytic hydrogen evolution activity of the Ni glyoximate functional core, the photocatalytic HER experiment using the model complex $Ni(dpg)_2$ as the catalyst was first performed. As shown in Figure 4a, hydrogen was detected in the presence of photosensitizer $Ru(bpy)_3^{2+}$. Considering the decent photocatalytic HER activity of Ni glyoximate core, intensive light absorption (photosensitive) and appropriate band structures, we envision that Ni-glyoximate-COFs might exhibit excellent performance for H_2 evolution. To verify this hypothesis, we then performed H_2 evolution experiments upon visible light illumination ($\lambda > 420$ nm) in water. As shown in Figure 4b, the HER yields of Ni-Py-COF and Ni-Bn-COF were 626 and 189 $\mu mol\, g^{-1} h^{-1}$ respectively under the above conditions without the addition of Pt co-catalyst. A possible mechanism is proposed in Figure S35. Ni-glyoximate-COFs absorb light energy and the electrons are excited from the VB to CB. Furthermore, the electrons are transferred to the Ni glyoximate cores and facilitate the reduction of protons to

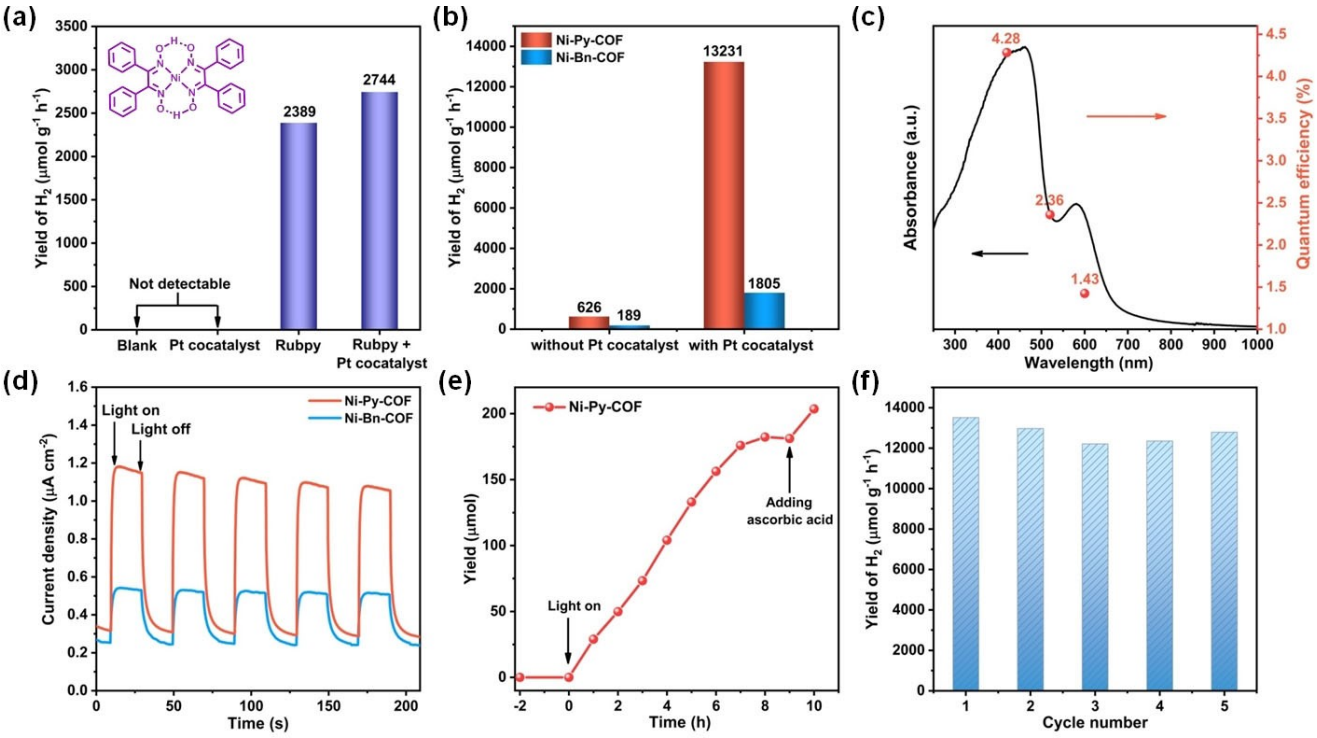

Figure 4. a) Photocatalytic H_2 evolution control experiments of $Ni(dpg)_2$. b) The photocatalytic performances of Ni-glyoximate-COFs without and with Pt cocatalyst in 10 mL water under visible ($\lambda > 420$ nm) light irradiation at 1 atm Ar. c) Wavelength-dependent AQE of photocatalytic H_2 evolution by Ni-Py-COF. d) Transient photocurrents measurements of Ni-glyoximate-COFs. e) Time dependent H_2 photogeneration using visible light for Ni-Py-COF. f) The photocatalytic recyclability of Ni-Py-COF.

H_2 on the acitve sites of O atoms (see Supporting Information for DFT calculation details and analysis). To further enhance the water splitting activity by lowering the H_2 evolution overpotential, Pt co-catalyst was introduced to the reaction system. The results showed that both the H_2 evolution activity of Ni-Py-COF and Ni-Bn-COF were remarkably increased with the HER reached up to 13231 and 1805 $\mu mol\, g^{-1} h^{-1}$, respectively. Importantly, the photocatalytic HER activity of Ni-Py-COF was superior to various porous organic photocatalysts (Table S4). Furthermore, we explored the influence of additional photosensitizer and found the addition of photosensitizer did not significantly improve the HER activity (Figure S23) for both COFs, indicating that the photosensitivity of Ni-glyoximate-COFs is sufficient to support the efficient photocatalysis. Moreover, the effect of the mass density of heterogeneous photocatalyst in solution on the HER performances was tested. The results demonstrated that 0.2 $mg\, mL^{-1}$ Ni-Py-COF was the optimized dosage under our test conditions (Figure S24). The HER yields presented downtrend when the content of Ni-Py-COF increased, which may be attributed to the shading effect that the utilization of light reduced as the dispersion concentration of COFs in the solvent increased.[23]

The apparent quantum efficiency (AQE) of Ni-Py-COF was calculated to quantify the photocatalytic activity for hydrogen evolution over the spectral distribution. The AQE, as a function of incident light wavelength, was measured using three different bandpass filters with central wavelengths of 420, 520 and 600 nm. It showed that the maximum AQE of Ni-Py-COF was 4.28 % at 420 nm (Figure 4c and S25), which is close to the maximum absorption peak.

Notably, Ni-Py-COF displayed significantly higher photocatalytic HER activity than Ni-Bn-COF. The reason for this huge difference might related to the conjugated structure and photogenerated electrons efficiency. Compared with Bn-4CHO, pyrene building units (Py-4CHO) show a planar structure which is conducive to stack closely and its extended π-conjugation is beneficial for the photogenerated charge carrier mobility.[24] To better understand the photoelectochemical properties of Ni-glyoximate-COFs, transient photocurrent responses, electrochemical impedance spectroscopy (EIS), steady-state photoluminescence (PL) spectra and time-resolved photoluminescence (TRPL) spectroscopy were conducted. As shown in Figure 4d, the photocurrent density of Ni-Py-COF was much higher than that of Ni-Bn-COF, indicating that Ni-Py-COF features faster photoresponse and induces better photoinduced charges transfer. The Nyquist impedance diagram of Ni-Py-COF displayed a smaller semicircle in comparison with Ni-Bn-COF (Figure S26), showing the lower internal charge transfer resistance in Ni-Py-COF that can achieve more efficient charges transportation. Additionally, compared with Ni-Bn-COF, the PL emission intensity of Ni-Py-COF displayed obvious quenching, suggesting that the recombination of photoexcited electrons and holes were more effectively inhibited (Figure S27). Meanwhile, the TRPL spectroscopy of Ni-Py-COF (Figure S28) exhibited faster decay kinetics and shorter fluorescence lifetime ($\tau_1 = 0.61$ ns, 61.4 %; $\tau_2 = 2.49$ ns, 38.6 % and $\tau_{avg} = 1.34$ ns) than that of Ni-Bn-COF ($\tau_1 = 0.77$ ns, 54.7 %; $\tau_2 = 3.14$ ns, 45.3 % and $\tau_{avg} = 1.85$ ns). The fitting results indicated that nonradiative recombination maybe the more dominant decay pathways, which is due to the fast electron transfer process from pyrene units to Ni glyoximate cores and the increase of nonradiative quenching pathways lead to a shorter decay lifetime of Ni-Py-COF. In summary, the obvious PL quenching and emission lifetime decrease suggested faster photo-induced charge transfer and more effective charge separation in Ni-Py-COF.[25] Moreover, the femtosecond transient absorption spectroscopy (fs-TAS) was employed to investigate the charge transfer kinetics. The significantly reduced lifetime of Ni-Py-COF ($\tau_{avg} = 1.7$ ns) compared with Py-4CHO ($\tau_{avg} = 6.9$ ns) confirmed the efficient electron transfer from pyrene units to active sites in Ni-Py-COF[26] (see Supporting Information Section 16 and Figure S29 for details and analysis). These characterizations identically revealed Ni-Py-COF is much superior to Ni-Bn-COF in photo-induced charge carriers separation and migration that is conducive to photocatalytic hydrogen evolution, which coincided with the experimental results.

The long-term stability in photocatalytic hydrogen production is a vital metric for photocatalysts. A time-dependent hydrogen evolution experiment that lasted for 10 h was conducted for Ni-Py-COF. The H_2 production exhibited continual increase tendency at the first 8 h and then saturated due to the depletion of sacrificial agent (Figure 4e). Hydrogen was reproduced again at a similar rate when ascorbic acid was readded into the system at the ninth hour. Subsequently, the cycling test was performed, and Ni-Py-COF maintained good photocatalytic stability after at least five cycles (Figure 4f). The PXRD (Figure S30), FT-IR (Figure S31), ssNMR (Figure S32) and SEM (Figure S33) results of the recycled Ni-Py-COF after photocatalysis indicated no obvious changes, thus supporting the favorable stability of Ni-Py-COF in the HER process. Moreover, highly dispersed Pt nanoparticles were observed by TEM (Figure S34), and the content of Pt was determined to be about 14 % by ICP-MS (Table S3).

In summary, we developed two Ni-glyoximate-COFs (Ni-Py-COF and Ni-Bn-COF) with a metal glyoximate functional core, which greatly enriched the diversity of MCOFs. Both Ni-glyoximate-COFs exhibited good photocatalytic performance for H_2 evolution due to the broad visible-light absorption and efficient charge separation. Furthermore, the photocatalytic activity and structural integrity were well maintained after cycling tests. Notably, the current work not only provides a new metalated functional building units for construction of MCOFs, but also displays a feasible strategy for photocatalytic H_2 evolution free of using noble metals. Furthermore, new glyoximate COFs with different built-in transition metals (e.g. Cu, Co, Pd, etc.) are currently in progress in our laboratory to further unravel the structure–property relationship at the molecular levels.

Acknowledgements

This work was financially supported by National Natural Science Foundation of China (51973153) and National Key Research and Development Program of China (2017YFA0207500).

Conflict of Interest

The authors declare no conflict of interest.

Data Availability Statement

The data that support the findings of this study are available in the Supporting Information of this article.

Keywords: Co-Catalysts · Metal–Covalent Organic Frameworks · Nickel Glyoximate · Photocatalytic Hydrogen Evolution

[1] a) K. Geng, T. He, R. Liu, S. Dalapati, K. T. Tan, Z. Li, S. Tao, Y. Gong, Q. Jiang, D. Jiang, *Chem. Rev.* **2020**, *120*, 8814–8933; b) T. Zhang, G. Zhang, L. Chen, *Acc. Chem. Res.* **2022**, *55*, 795–808.

[2] a) M. Li, J. Liu, Y. Li, G. Xing, X. Yu, C. Peng, L. Chen, *CCS Chem.* **2020**, *2*, 696–706; b) X. Wang, P. She, Q. Zhang, *SmartMat* **2021**, *2*, 299–325.

[3] a) Y. Lv, Y. Li, G. Zhang, Z. Peng, L. Ye, Y. Chen, T. Zhang, G. Xing, L. Chen, *CCS Chem.* **2021**, *3*, 1773–1779; b) H. Qi, B. Liang, U. Kaiser, *SmartMat* **2021**, *2*, 131–138.

[4] J. Dong, X. Han, Y. Liu, H. Li, Y. Cui, *Angew. Chem. Int. Ed.* **2020**, *59*, 13722–13733; *Angew. Chem.* **2020**, *132*, 13826–13837.

[5] a) S. Lin, C. S. Diercks, Y.-B. Zhang, N. Kornienko, E. M. Nichols, Y. Zhao, A. R. Paris, D. Kim, P. Yang, O. M. Yaghi, C. Chang, *Science* **2015**, *349*, 1208–1213; b) R. Chen, Y. Wang, Y. Ma, A. Mal, X.-Y. Gao, L. Gao, L. Qiao, X.-B. Li, L.-Z. Wu, C. Wang, *Nat. Commun.* **2021**, *12*, 1354; c) C. S. Diercks, S. Lin, N. Kornienko, E. A. Kapustin, E. M. Nichols, C. Zhu, Y. Zhao, C. J. Chang, O. M. Yaghi, *J. Am. Chem. Soc.* **2018**, *140*, 1116–1122; d) W. Liu, X. Li, C. Wang, H. Pan, W. Liu, K. Wang, Q. Zeng, R. Wang, J. Jiang, *J. Am. Chem. Soc.* **2019**, *141*, 17431–17440; e) Y. Meng, Y. Luo, J.-L. Shi, H. Ding, X. Lang, W. Chen, A. Zheng, J. Sun, C. Wang, *Angew. Chem. Int. Ed.* **2020**, *59*, 3624–3629; *Angew. Chem.* **2020**, *132*, 3653–3658; f) H.-J. Zhu, M. Lu, Y.-R. Wang, S.-J. Yao, M. Zhang, Y.-H. Kan, J. Liu, Y. Chen, S.-L. Li, Y.-Q. Lan, *Nat. Commun.* **2020**, *11*, 497; g) Y. Qian, D. Li, Y. Han, H.-L. Jiang, *J. Am. Chem. Soc.* **2020**, *142*, 20763–20771.

[6] a) J. Huang, X. Han, S. Yang, Y. Cao, C. Yuan, Y. Liu, J. Wang, Y. Cui, *J. Am. Chem. Soc.* **2019**, *141*, 8996–9003; b) Y. Liu, Y. Ma, Y. Yang, C. S. Diercks, N. Tamura, F. Jin, O. M. Yaghi, *J. Am. Chem. Soc.* **2018**, *140*, 16015–16019.

[7] a) M. Wang, M. Ballabio, M. Wang, H.-H. Lin, B. P. Biswal, X. Han, S. Paasch, E. Brunner, P. Liu, M. Chen, et al., *J. Am. Chem. Soc.* **2019**, *141*, 16810–16816; b) X. Ding, J. Guo, X. Feng, Y. Honsho, J. Guo, S. Seki, P. Maitarad, A. Saeki, S. Nagase, D. Jiang, *Angew. Chem. Int. Ed.* **2011**, *50*, 1289–1293; *Angew. Chem.* **2011**, *123*, 1325–1329.

[8] Z. Meng, R. M. Stolz, K. A. Mirica, *J. Am. Chem. Soc.* **2019**, *141*, 11929–11937.

[9] a) X. Han, Q. Xia, J. Huang, Y. Liu, C. Tan, Y. Cui, *J. Am. Chem. Soc.* **2017**, *139*, 8693–8697; b) T. Li, W.-D. Zhang, Y. Liu, Y. Li, C. Cheng, H. Zhu, X. Yan, Z. Li, Z.-G. Gu, *J. Mater. Chem. A* **2019**, *7*, 19676–19681.

[10] Z. Wang, C. Li, K. Domen, *Chem. Soc. Rev.* **2019**, *48*, 2109–2125.

[11] a) S. Wang, G. Liu, L. Wang, *Chem. Rev.* **2019**, *119*, 5192–5247; b) C. Zhao, Z. Chen, R. Shi, X. Yang, T. Zhang, *Adv. Mater.* **2020**, *32*, 1907296.

[12] a) L. Stegbauer, K. Schwinghammer, B. V. Lotsch, *Chem. Sci.* **2014**, *5*, 2789–2793; b) V. S. Vyas, F. Haase, L. Stegbauer, G. Savasci, F. Podjaski, C. Ochsenfeld, B. V. Lotsch, *Nat. Commun.* **2015**, *6*, 8508; c) F. Haase, T. Banerjee, G. Savasci, C. Ochsenfeld, B. V. Lotsch, *Faraday Discuss.* **2017**, *201*, 247–264; d) X. Wang, L. Chen, S. Y. Chong, M. A. Little, Y. Wu, W.-H. Zhu, R. Clowes, Y. Yan, M. A. Zwijnenburg, R. S. Sprick, A. I. Cooper, *Nat. Chem.* **2018**, *10*, 1180–1189; e) P. Pachfule, A. Acharjya, J. Roeser, T. Langenhahn, M. Schwarze, R. Schomäcker, A. Thomas, J. Schmidt, *J. Am. Chem. Soc.* **2018**, *140*, 1423–1427; f) S. Wei, F. Zhang, W. Zhang, P. Qiang, K. Yu, X. Fu, D. Wu, S. Bi, F. Zhang, *J. Am. Chem. Soc.* **2019**, *141*, 14272–14279; g) W. Chen, L. Wang, D. Mo, F. He, Z. Wen, X. Wu, H. Xu, L. Chen, *Angew. Chem. Int. Ed.* **2020**, *59*, 16902–16909; *Angew. Chem.* **2020**, *132*, 17050–17057.

[13] a) Z. H. N. Al-Azri, V. Jovic, W.-T. Chen, D. Sun-Waterhouse, J. B. Metson, G. I. N. Waterhouse, *Int. J. Nanotechnol.* **2014**, *11*, 695–703; b) S. V. Awate, S. S. Deshpande, K. Rakesh, P. Dhanasekaran, N. M. Gupta, *Phys. Chem. Chem. Phys.* **2011**, *13*, 11329–11339; c) X.-H. Jiang, L.-S. Zhang, H.-Y. Liu, D.-S. Wu, F.-Y. Wu, L. Tian, L.-L. Liu, J.-P. Zou, S.-L. Luo, B.-B. Chen, *Angew. Chem. Int. Ed.* **2020**, *59*, 23112–23116; *Angew. Chem.* **2020**, *132*, 23312–23316.

[14] a) X. Liu, H. Zhuang, *Int. J. Energy Res.* **2021**, *45*, 1480–1495; b) J. Huo, Y.-B. Zhang, W.-Y. Zou, X. Hu, Q. Deng, D. Chen, *Catal. Sci. Technol.* **2019**, *9*, 2716–2727; c) L.-S. Zhang, X.-H. Jiang, Z.-A. Zhong, L. Tian, Q. Sun, Y.-T. Cui, X. Lu, J.-P. Zou, S.-L. Luo, *Angew. Chem. Int. Ed.* **2021**, *60*, 21751–21755; *Angew. Chem.* **2021**, *133*, 21919–21923.

[15] L. Tschugaeff, *Ber. Dtsch. Chem. Ges.* **1905**, *38*, 2520–2522.

[16] A. Kilic, M. Durgun, E. Tas, I. Yilmaz, *Transition Met. Chem.* **2008**, *33*, 29–37.

[17] M. Cowie, A. Gleizes, G. W. Grynkewich, D. W. Kalina, M. S. McClure, R. P. Scaringe, R. C. Teitelbaum, S. L. Ruby, J. A. Ibers, C. R. Kannewurf, T. J. Marks, *J. Am. Chem. Soc.* **1979**, *101*, 2921–2936.

[18] a) S.-W. Cao, Y.-P. Yuan, J. Barber, S. C. J. Loo, C. Xue, *Appl. Surf. Sci.* **2014**, *319*, 344–349; b) R. Wang, L. Wu, B. Chica, L. Gu, G. Xu, Y. Yuan, *J. Materiomics* **2017**, *3*, 58–62.

[19] L. S. Xie, S. S. Park, M. J. Chmielewski, H. Liu, R. A. Kharod, L. Yang, M. G. Campbell, M. Dincă, *Angew. Chem. Int. Ed.* **2020**, *59*, 19623–19626; *Angew. Chem.* **2020**, *132*, 19791–19794.

[20] a) J. Yu, S. Wang, B. Cheng, Z. Lin, F. Huang, *Catal. Sci. Technol.* **2013**, *3*, 1782–1789; b) J. Yan, H. Wu, H. Chen, L. Pang, Y. Zhang, R. Jiang, L. Li, S. Liu, *Appl. Catal. Environ.* **2016**, *194*, 74–83; c) X. Lu, J. Xie, S.-Y. Liu, A. Adamski, X. Chen, X. Li, *ACS Sustainable Chem. Eng.* **2018**, *6*, 13140–13150; d) M. Hojamberdiev, M. M. Khan, Z. Kadirova, K. Kawashima, K. Yubuta, K. Teshima, R. Riedel, M. Hasegawa, *Renewable Energy* **2019**, *138*, 434–444.

[21] a) J. Qin, B. Wang, X. Zhang, X. Zhang, *J. Nanosci. Nanotechnol.* **2012**, *12*, 6592–6595; b) E. Taş, A. Çukurovali, M. Kaya, *J. Coord. Chem.* **1998**, *44*, 109–117; c) B. Yildirim, E. Özcan, P. Deveci, *Russ. J. Coord. Chem.* **2007**, *33*, 417–421.

[22] a) S. Zhang, G. Cheng, L. Guo, N. Wang, B. Tan, S. Jin, *Angew. Chem. Int. Ed.* **2020**, *59*, 6007–6014; *Angew. Chem.*

2020, *132*, 6063–6070; b) S. Wang, B. Y. Guan, X. Wang, X. W. D. Lou, *J. Am. Chem. Soc.* **2018**, *140*, 15145–15148.

[23] L. Xiao, T. Su, Z. Wang, K. Zhang, X. Peng, Y. Han, Q. Li, X. Wang, *Nanoscale Res. Lett.* **2018**, *13*, 31–40.

[24] a) Y. Xu, C. Zhang, P. Mu, N. Mao, X. Wang, Q. He, F. Wang, J.-X. Jiang, *Sci. China Chem.* **2017**, *60*, 1075–1083; b) C. Dai, S. Xu, W. Liu, X. Gong, M. Panahandeh-Fard, Z. Liu, D. Zhang, C. Xue, K. P. Loh, B. Liu, *Small* **2018**, *14*, 1801839; c) J.-Z. Cheng, Z.-R. Tan, Y.-Q. Xing, Z.-Q. Shen, Y.-J. Zhang, L.-L. Liu, K. Yang, L. Chen, S.-Y. Liu, *J. Mater. Chem. A* **2021**, *9*, 5787–5795.

[25] a) S. Cao, B. Shen, T. Tong, J. Fu, J. Yu, *Adv. Funct. Mater.* **2018**, *28*, 1800136; b) T.-C. Zhuo, Y. Song, G.-L. Zhuang, L.-P. Chang, S. Yao, W. Zhang, Y. Wang, P. Wang, W. Lin, T.-B. Lu, Z.-M. Zhang, *J. Am. Chem. Soc.* **2021**, *143*, 6114–6122; c) S. Wang, B. Y. Guan, X. W. D. Lou, *J. Am. Chem. Soc.* **2018**, *140*, 5037–5040; d) D. Hollmann, M. Karnahl, S. Tschierlei, K. Kailasam, M. Schneider, J. Radnik, K. Grabow, U. Bentrup, H. Junge, M. Beller, S. Lochbrunner, A. Thomas, A. Brückner, *Chem. Mater.* **2014**, *26*, 1727–1733; e) V. W. Lau, V. W. Yu, F. Ehrat, T. Botari, I. Moudrakovski, T. Simon, V. Duppel, E. Medina, J. K. Stolarczyk, J. Feldmann, V. Blum, B. V. Lotsch, *Adv. Energy Mater.* **2017**, *7*, 1602251.

[26] Z.-H. Yan, M.-H. Du, J. Liu, S. Jin, C. Wang, G.-L. Zhuang, X.-J. Kong, L.-S. Long, L.-S. Zheng, *Nat. Commun.* **2018**, *9*, 3353.

Manuscript received: March 23, 2022
Accepted manuscript online: May 13, 2022
Version of record online: June 8, 2022